Probing the Mechanism of Structure-Switching Aptamer Assembly by Super-Resolution Localization of Individual DNA Molecules

Hershel H. Lackey,[†#] Eric M. Peterson,[†#] Joel M. Harris,[†*] and Jennifer M. Heemstra[†‡*]

[†] Department of Chemistry, University of Utah, Salt Lake City, UT, 84112, USA
[‡] Department of Chemistry, Emory University, Atlanta, GA, 30322, USA

* Address correspondence to Joel M. Harris and Jennifer M. Heemstra:
harrisj@chem.utah.edu, 801-581-3585 and jen.heemstra@emory.edu, 404-727-7766

# The first authors contributed equally to this manuscript.

Abstract

Oligonucleotide aptamers can be converted into structure-switching biosensors by incorporating a short, typically-labeled oligonucleotide that is complementary to the analyte-binding region. Binding of a target analyte can disrupt the hybridization equilibrium between the aptamer and the labeled-complementary oligo producing a concentration-dependent signal for target-analyte sensing. Despite its importance in the performance of a biosensor, the mechanism of analyte-response of most structure-switching aptamers is not well understood. In this work, we employ single-molecule fluorescence imaging to investigate the competitive kinetics of association of a labeled complementary oligonucleotide and a target analyte, L-tyrosinamide (L-Tym), interacting with an L-Tym-binding aptamer. The complementary readout strand is fluorescently labeled, allowing us to measure its hybridization kinetics with *individual aptamers* immobilized on a surface and located with super-resolution techniques; the small-molecule L-Tym analyte, is *not labeled* in order to avoid having an attached dye molecule impact its interactions with the aptamer. We measure the association kinetics of *unlabeled* L-Tym by detecting its influence on the hybridization of the *labeled* complementary strand. We find that L-Tym slows the association rate of the complementary strand with the aptamer but does not impact its dissociation rate, suggesting an S_N1-like mechanism where the complementary strand must dissociate before L-Tym can bind. The competitive model revealed a slow association rate between L-Tym and the aptamer, producing a long-lived L-Tym-aptamer complex that blocks hybridization with the labeled complementary strand. These results provide insight about the kinetics and mechanism of analyte recognition in this structure-switching aptamer, and the methodology provides a general means of measuring rates of *unlabeled-analyte binding kinetics* in aptamer-based biosensors.

INTRODUCTION

Structure-switching aptamers hold promise as rapid, sensitive biosensors for biomedical and environmental applications.[1-2] These affinity reagents take advantage of the unique ability of nucleic acids to form Watson-Crick-Franklin base pairs and adopt 3D configurations that not only bind target analytes with high affinity and specificity, but can also undergo a change in conformation or accessibility upon target binding.[3] A common structure-switching or duplexed aptamer biosensor uses a short oligonucleotide "complementary strand" that is hybridized to the aptamer and can be displaced by the conformation change induced upon introduction of ligand. Dissociation of the short complementary strand can produce a variety of signal responses including fluorescence,[4-5] colormetric,[6] and electrochemical,[7] which can be used to quantify the concentration of ligand. Aptamers can be generated through SELEX against a broad target scope including cells, proteins, ions, and small molecules,[8] and selection methods can be tailored to select aptamers that undergo the large conformation changes required for use in structure-switching biosensors.[9] Recent advances in SELEX include an expanded genetic alphabet,[10] non-natural sugar backbones,[11-12] and incorporation of amino acid-like side chains,[13-15] offering the promise of sensors having high affinity, specificity, and nuclease resistance.

Changing the length and position of the complementary strand affects the equilibrium between the aptamer, complementary strand, and ligand, allowing the dynamic range and sensitivity of the aptamer biosensor to be optimized.[2, 16-18] For instance, if an immobilized aptamer biosensor undergoes an S_N2-like mechanism (Scheme 1A), where ligand binding and displacement of complementary strand are concerted, a complementary strand with a slow-dissociation rate and a high susceptibility to strand invasion would minimize background signal and improve sensitivity. On the other hand, if the aptamer undergoes an S_N1-like (Scheme 1B) mechanism, in which the complementary strand must first dissociate before the target can bind, then a complementary strand having a fast dissociation rate would

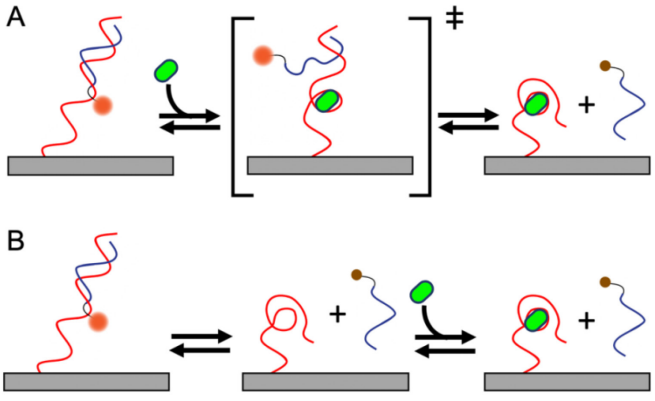

Scheme 1. Kinetics of an immobilized structure-switching aptamer. (A) S_N2-like, where target analyte (green-oval) binds to aptamer (red-strand), destabilizing the complement-aptamer duplex (braces), leading to concerted dissociation and loss of fluorescence from the labeled-complement as it diffuses from the interfacial-excitation region. (B) S_N1-like, where labeled-compliment first dissociates from the aptamer and then target binding can occur.

increase the response time and sensitivity. To understand the aptamer response mechanism, we need analytical techniques to measure the underlying kinetics, thermodynamics, and mechanism of aptamer-ligand and aptamer-complementary-strand interactions.

Single-molecule fluorescence imaging methods[19-23] have demonstrated high selectivity and sensitivity in DNA detection assays[24-25] and provide insight into population heterogeneity, reversible kinetic processes at equilibrium, and details about statistical distributions of molecular events that are lost in an ensemble average typical of less sensitive analytical techniques. These methods have been adapted to study structure-switching aptamers, such as the adenosine[19-20] and cocaine[26] binding aptamer. In the present work, we address the response mechanism question raised in Scheme 1 for the L-tyrosinamide (L-Tym) structure-switching aptamer.[27] We address this question by using single-molecule imaging to characterize the equilibrium and kinetics of *both the labeled complementary strand and the unlabeled small molecule ligand*, applying a competitive kinetics model for competitive DNA hybridization.[28] This small molecule-binding aptamer biosensor is adapted to a surface-based single-molecule assay to study the kinetics of both the complementary strand and the small molecule target interacting with the aptamer (Scheme 1). Individual L-Tym aptamer molecules are immobilized at the surface of a glass coverslip with *no fluorescent label*, so they are not susceptible to photobleaching and can be observed for long periods of time. The complementary readout strand in solution is labeled with a Cy3 fluorescent dye, so that hybridization with the aptamer results in detectable single-molecule fluorescence spots on the glass surface. Aptamer molecules on the surface are located by identifying sites of repeated hybridization events with the labeled-complementary readout strand using super-resolution or sub-diffraction imaging techniques to map their locations.[21-23] This methodology allows a nearly 20-fold greater population of immobilized aptamers to be observed within the field of view, increasing the rate of data collection by a similar factor; more importantly, super-resolution provides better spatial resolution of active sites to discriminate against non-specific surface interactions.[28-31] Hybridization kinetics are determined for each aptamer molecule by monitoring the times required for the labeled complementary strand to associate and dissociate. L-Tym competes with the complementary strand to bind to the aptamer, altering the intervals between complementary-strand hybridization events. The L-Tym analyte is not labeled since a fluorophore attached to a small target molecule can significantly perturb its binding affinity with the aptamer.[32]

Although fluorescent labels conjugated with DNA have been shown to affect the thermodynamics[33-34] and kinetics[28] of DNA hybridization, their use is directly applicable to

structure-switching aptamer biosensors where they are often used to facilitate readout. While the kinetics of the complementary-strand association with the aptamer include the influence of a dye label, the kinetics of unlabeled L-Tym binding to the aptamer are not monitored without a label, but are instead determined from changes in time-intervals between the labeled complementary-strand hybridization with individual immobilized aptamers on the surface. This measurement approach can allow one to detect the influence of non-fluorescent molecules on the site-binding kinetics of fluorescent molecules; this concept was pioneered in recent research, where catalytic sites for generation of a fluorescent product were located and monitored, and non-fluorescent reactions that compete for access to these catalytic sites were observed.[35] In the present work, we apply this concept to measuring competitive association of immobilized L-Tym-aptamer with its unlabeled L-Tym target and a labeled-complementary readout strand by applying a kinetic model recently developed to determine the hybridization kinetics of *unlabeled* DNA.[28]

The trend in the complementary-strand on-rate at varying concentrations of L-Tym follows the competitive-kinetic model[28] and reveals both the association and dissociation rates of L-Tym with the aptamer, which are similar to rates measured for a free-solution variant of the L-Tym aptamer.[36] Measurements at varying L-Tym concentrations revealed a population of aptamers that hybridize with the complementary strand, but have no measurable response to L-Tym. Identifying and excluding this population of inactive aptamers shows the unique capabilities of an individual-molecule analysis relative to ensemble methods[30, 37] and likely explains the lack of full fluorescence-recovery response previously seen in solution-phase L-Tym aptamer assays.[27] The results indicate that the structure-switching mechanism of the aptamer is a purely competitive S_N-1 scheme, where the complementary strand must dissociate before the target ligand can bind and vice versa.

EXPERIMENTAL SECTION

Super-Resolution Single-molecule TIRF imaging and data analysis. PEG-biotin modified substrates (Supporting Information) were loaded into an imaging microfluidics flow cell to allow introduction of samples for fluorescence imaging, as described previously.[38] Fluorescently-labeled oligonucleotides (Supporting Information) were detected at the glass-solution interface using a total-internal reflection fluorescence microscope with through-the-objective illumination (Supporting Information). The microscope was enclosed in a temperature-controlled chamber fixed at 23±0.2°C. Image stacks were collected with time-lapse exposures of 100-ms in 500-ms intervals using a slow readout speed (1-MHz) in order to reduce camera read

noise. Laser exposure was 54-Wcm^{-2} during the 100-ms exposure time. In previous work, we observed minimal photobleaching of Cy3 fluorophores over the lifetime of the duplex (~5 s in this case) using similar laser exposure.[29] In this current work, we employ an enzymatic oxygen-scavenging buffer, which has been shown to further reduce photobleaching.[39-40] The length of the video stacks was varied from 10 to 50 min depending on the apparent on-rate of complementary strand hybridization (which decreased with increasing L-Tym concentration) to ensure that a similar average of 8 or more hybridization events were observed at each aptamer molecule. Images were collected with a 300x300-pixel cropped region of the sensor, corresponding to a 50x50-μm field-of-view at the sample plane. Images were collected using Andor SOLIS software version 4.27.30001.0 as monochrome 16bit FITS image stacks. Images were analyzed with super-resolution techniques by locating the centroid of individual single-molecule spots and fitting a 2D Gaussian function to the intensity point-spread function.[29] Sample drift was corrected using a spatial-temporal cross correlation analysis that tracks concerted changes in the locations of aptamer-complementary-strand duplexes.[41] Corrected coordinates were tracked in time to determine the arrival time and duration of individual hybridization events with the aptamer, and clusters of events were grouped together to locate and calculate average association and dissociation rates for each individual aptamer-molecule binding sites. Uncertainties in plots of the association and dissociation rates are reported as 90% confidence bounds on the determined variations in rates with complementary-strand or L-Tym concentration.

RESULTS AND DISCUSSION

Fluorescence imaging and mapping of aptamer-binding sites. Aptamers were immobilized onto substrates as illustrated in Supporting Information, Scheme S1. Substrates modified with biotin are incubated in an imaging flow cell with 10-nM streptavidin solution to generate capture sites. A mixture of dilute biotin-modified aptamers and Cy3-labeled complementary strand is then injected into the flow cell while imaging the substrate. The DNA aptamer is captured at the surface through a biotin-streptavidin binding interaction,[42] while monitoring the buildup by detecting the fluorescent complementary strand that simultaneously undergoes reversible hybridization with the aptamer. Once the aptamer density reaches ~300 complementary-strand molecules, accumulation is halted by rinsing with imaging buffer solution. Rinsing removes unbound biotin-aptamer and weakly-hybridized complementary strand, while retaining the immobilized DNA aptamer due to the slow dissociation of the biotin-streptavidin interaction (lifetime~50 h).[43]

The immobilized aptamer molecules are located by tracking the arrival of fluorescent complementary strands using DNA point-accumulation-imaging-of-nanoscale-topology or DNA-PAINT,[21-23] where complementary strands stochastically visit specific locations on the surface as a result of reversible hybridization at individual immobilized aptamer molecules. Fluorescent spots corresponding to individual molecules are located in images by defining a region-of-interest around intense spots (see Figure S1) and fitting a 2D-Gaussian point-spread function to its intensity profile to locate precisely its centroid coordinate.[29] These localized molecular coordinates are then spatially-temporally correlated to measure stage drift during the video acquisition time.[41] Drift-corrected coordinates are tracked in time to determine the location, arrival time, and duration of each binding "event." By plotting the locations of individual molecular events on spatial-histogram map (Figure 1A), we observe tightly clustered regions on the aptamer-modified surface that show high affinity for complementary DNA, with each cluster, typically made up of more than 20 localized events whose variation in event density is consistent with a Poisson distribution.[29] There are also randomly dispersed events in Figure 1A characteristic of non-specific interactions, and these random events are also observed when the aptamer-modified surface is exposed to a labeled non-complementary sequence probe (Figure S2).

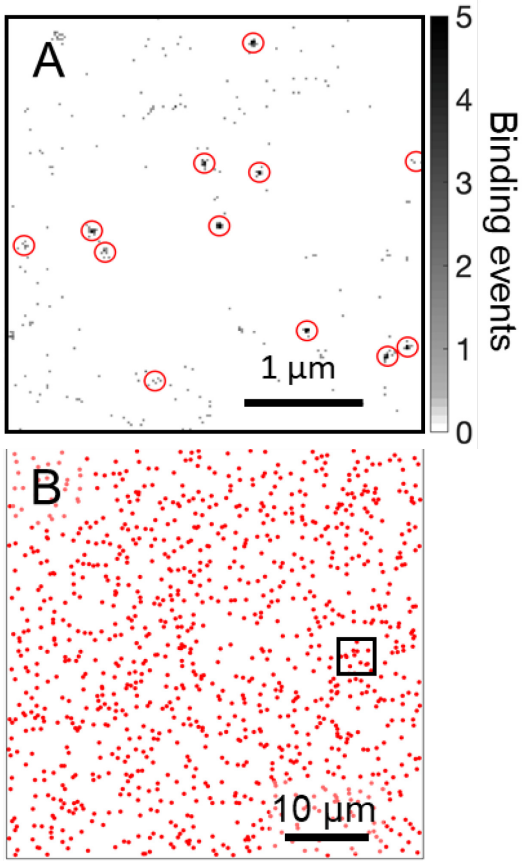

Figure 1. Map of labeled-complement DNA binding events. A) 2D gray-scale histogram of the number of events detected at each location over 10 min in 1200 video frames. Clusters of events that meet both spatial and kinetic criteria, described in the section below, are designated as aptamer binding sites, circled in red. B) Map of the 1081 binding sites (red) in 50x50-µm field of view, where the small box designates the magnified region shown in A.

Spatial and kinetic criteria to identify binding sites. To identify aptamer binding sites and distinguish these from non-specific interactions, both spatial and kinetic criteria were applied to determine the locations where multiple events occur and whether the events exhibit a relevant kinetic signature. Binding sites were first screened spatially to determine clusters of events in the drift-corrected maps that have three or more events within an 80-nm radius. This size was based on a measurement of the localization precision from the distribution of binding events around the

center (spatial-mean) of each cluster (see Figure S3). The resulting spatial precision is 39-nm, a radius that includes 95% of the binding events within each cluster. To assure >99% confidence for event-detection at each aptamer site, a conservative criterion of r = 80-nm for identifying event clusters (Figure S3). This sub-diffraction resolution criterion represents a 17-fold smaller area than the diffraction-limited spots in the image, significantly reducing the influence of non-specific interactions on the analysis of complementary strand association events.[30]

While sub-diffraction spatial criteria are valuable for identifying complementary-strand hybridization at individual aptamer sites, non-specific interactions can occasionally form clusters of ~5 events per video stack, likely arising from interactions with defect sites on the surface. To further distinguish specific aptamer hybridization from nonspecific events, we turn to the "kinetic fingerprinting" methodology developed by Johnson-Buck and coworkers,[42] in which the kinetic behavior of individual capture sites is used to distinguish nonspecific adsorption from sequence-specific hybridization. We have added two kinetic criteria to reject site clusters dominated by nonspecific adsorption:[29] first, clusters exhibiting weak complementary-strand affinity, where more than half of the binding events appear only in a single-video frame are eliminated; second, to reject transient non-specific interactions, acceptable sites must display binding events throughout the 10-min video, with at least one event in both the first and last 3 minutes of accumulation. The aptamer binding sites thus selected on the basis of spatial and kinetic criteria are circled in red in Figure 1A, with the full frame of identified sites in Figure 1B.

Kinetics of complementary-strand hybridization to aptamer sites. Having screened sites based on spatial and kinetic criteria, the arrival and departure time stamp of each labeled-complement-binding event can be used generate an "occupancy" trajectory that indicates the labeled-complement-binding status of each site. The occupancy trajectories show good agreement with the fluorescence intensity trajectories that are typically used to determine the site occupancy, shown in Figure S4A-C. A significant advantage of tracking the locations molecular events over monitoring raw intensity is that trajectories are not affected by fluorescence intensity spilling over from point-spread-functions of nearby molecules.

With non-complementary strands, most trajectories have rare short-lived "on" states, and long "off" states as shown in Figure S4A. With the complementary strand, binding sites show more frequent on-off fluorescence cycling due to reversible hybridization. Since the occupancy trajectories determined from site-tracking are discrete, it is trivial to measure the number, n_i, of each on- and off-state at each site of duration, i, in video frames. The characteristic rate of each

molecule can be determined from the inverse of a maximum-likelihood-estimate (MLE) of the event durations, based on the minimum time bin collected, j, the interval between video frames, T, and the total number of events, N.[29]

$$\hat{k} = \left[\frac{T}{N}\sum_{i=j}^{i=\infty} i\, n_i - (j - 1/2)\right]^{-1} \qquad \textbf{Equation 1}$$

In other words, the MLE rates of complementary-strand (CS) association and dissociation, $\hat{k'}_{on,CS}$ and $\hat{k}_{off,CS}$, are the inverse of the average of all sampled lifetimes with a small offset to correct bias due to the width of the first bin. Note that $\hat{k'}_{on,CS}$ (with a prime) is a pseudo-first-order association rate or on-rate in s^{-1}, where $k'_{on,CS} = k_{on,CS}\,[CS]$. Two dimensional histograms of the $\hat{k'}_{on,CS}$ and $\hat{k}_{off,CS}$ at all detected binding sites are shown for the non-complementary and complementary strands in Figures 2A and 2B, respectively. The distribution of rates for non-complementary "sites" are dispersed and noisy (Figure 2A), while the complementary strand shows a single cluster of aptamer sites with on-rates and off-rates of $k'_{on,CS}$~0.05±0.02 s^{-1} and $k_{off,CS}$~0.2±0.06 s^{-1} (Figure 2B). The width of the single-site-kinetics distributions are governed by statistical uncertainty from the relatively low number of hybridization events sampled, typically ~20 events where the rate of event arrivals is given by $(1/k'_{on,CS} + 1/k_{off,CS})^{-1}$, and heterogeneity in the kinetics due to molecule-to-molecule differences and variations over time due to temperature drift and the large enthalpy of hybridization.[44] By modeling the statistical contributions using an Erlang distribution,[29] we estimate that for the 30% site-to-site relative standard deviation of $k'_{on,CS}$ and

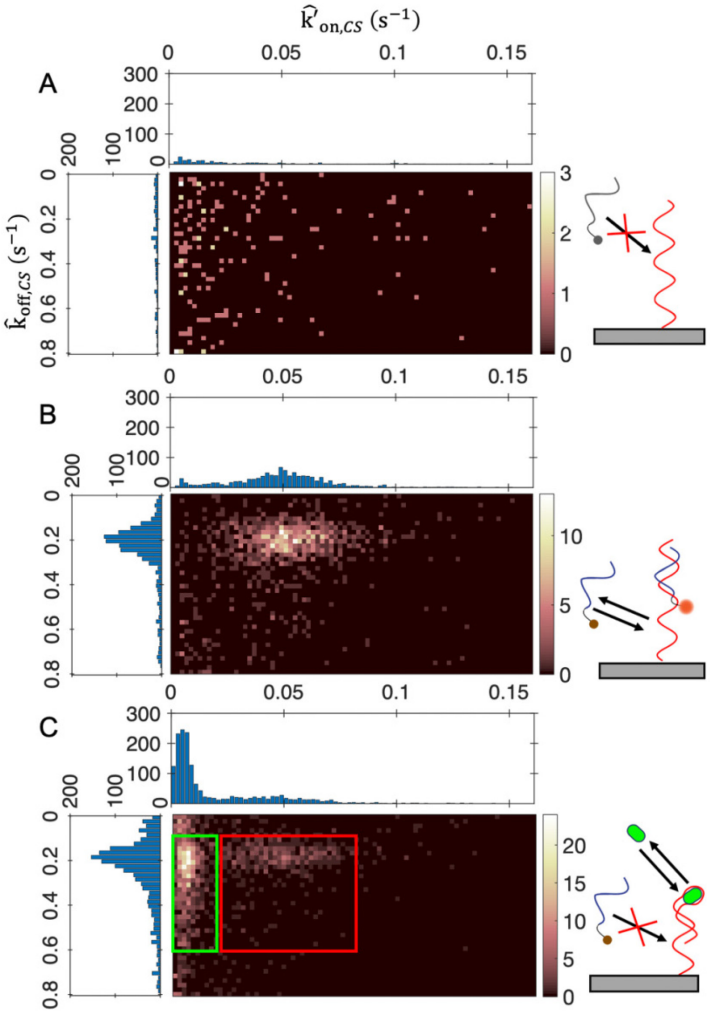

Figure 2. Identifying aptamer sites by kinetic fingerprinting. MLE association and dissociation rates are plotted as 2-D histograms at sites having ≥3 events for the following samples: (A) immobilized aptamer with 10-nM non-complementary strand, (B) aptamer with 10-nM fully-complementary strand, and (C) aptamer with 10-nM fully-complementary strand and 27-μM L-Tym. Sites whose kinetics are within the boxes shown in C are selected and used as reference sites to identify 'active' (green) and 'inactive' (red) aptamers in other data sets.

$k_{off,CS}$, ~20% is due to sampling statistics and ~20% due to sample heterogeneity. We have previously shown[29] that similar sample heterogeneity has minimal impact on the accuracy of rates determined by averaging the kinetics from a thousand sites within the field-of-view of the measurement (Figure 1B).

Competitive binding of the complementary strand and L-Tym to the immobilized aptamer. Having shown that we can detect specific hybridization between the complementary strand and aptamer, we next investigate the influence of L-Tym on the complementary-strand hybridization kinetics. Hybridization rates were measured for samples containing mixtures of constant complementary strand and varying L-Tym concentration in oxygen-scavenging buffer. A 2-D association-dissociation rate histogram of sites with 27-μM L-Tym and 10-nM complementary strand is shown in Figure 2C. In the presence of L-Tym, the distribution of hybridization kinetics shows two peaks; one population has a slower on-rate, $k'_{on,CS}$ ~0.008 s^{-1}, while the other population has a similar rate, $k'_{on,CS}$ ~0.05 s^{-1}, to the sample with no L-Tym. This result shows that a fraction of the aptamers exhibit hindered association with the complementary strand as a result of interactions with L-Tym, while the remaining aptamers exhibit unhindered association with the complementary strand. We have separated these populations of aptamers based on their on-rates using statistical criteria described in Figure S5. In the presence of 27-μM L-Tym, those aptamers with $k'_{on,CS} > 0.02$ s^{-1}, are defined as "active" aptamers, representing ~70% of the population, while those with higher $k'_{on,CS}$ are "inactive" aptamers (Figures 2C and S5). Inactive aptamers have the same association and dissociation kinetics in the presence and absence of L-Tym (Figure S6, S7). Additionally, the aptamers do not interconvert on the time-scale of these experiments; identified active and inactive aptamers exhibit equivalent sensitivity to L-Tym and rate distributions in videos collected hours apart. Therefore, individual active and inactive aptamer molecules located in samples with high L-Tym concentration can be tracked across samples with varying L-Tym concentration to determine how target binding affects duplex formation.

"Active" aptamers exhibit competitive binding between complementary strand and L-Tym. The active aptamer population was monitored at varying L-Tym concentrations to systematically probe how binding between the aptamer and target analyte influences the hybridization kinetics of the complementary strand. With L-Tym concentrations between 0- and 50-μM, the apparent association-rates, $\boldsymbol{k_{on,CS}^{app}}$ and off rates, $\boldsymbol{k_{off,CS}}$, of the complementary strand were calculated from the average lifetime of the *N* binding events measured at all filtered aptamer sites:

$$\boldsymbol{k_{on,CS}^{app} = \left(\frac{[CS]}{N}\sum \boldsymbol{\tau_{on}}\right)^{-1}}$$

$$k_{off,CS} = \left(\frac{1}{N}\sum \tau_{off}\right)^{-1} \quad \textbf{Equation 2}$$

As shown in Figure 3, the association rate decreases with increasing L-Tym concentration while the off-rate does not significantly change, the latter result being is consistent with an SN1-like competitive binding where L-Tym does not invade the duplex and increase the dissociation rate. Since L-Tym does not induce dissociation, the trend in $k_{on,CS}^{app}$with [L-Tym] can be interpreted using a simple equilibrium model, where the fraction of time that aptamers are occupied by L-Tym is governed by their concentration and dissociation constant of an aptamer-L-Tym complex, $K_{d,LTym}$:

$$\theta = \frac{[LTym]}{[LTym]+K_{d,LTym}} \quad \textbf{Equation 3}$$

If we assume that aptamers bound to L-Tym are unavailable for hybridization with complementary strand, then $k_{on,CS}^{app}$ will be equal to the native association-rate, $k_{on,CS}$, multiplied by the fraction of time aptamers are *not* bound to L-Tym, (*1-θ*):

$$k_{on,CS}^{app} = k_{on,CS}\left(1 - \frac{[LTym]}{[LTym]+K_{d,LTym}}\right)$$

Equation 4

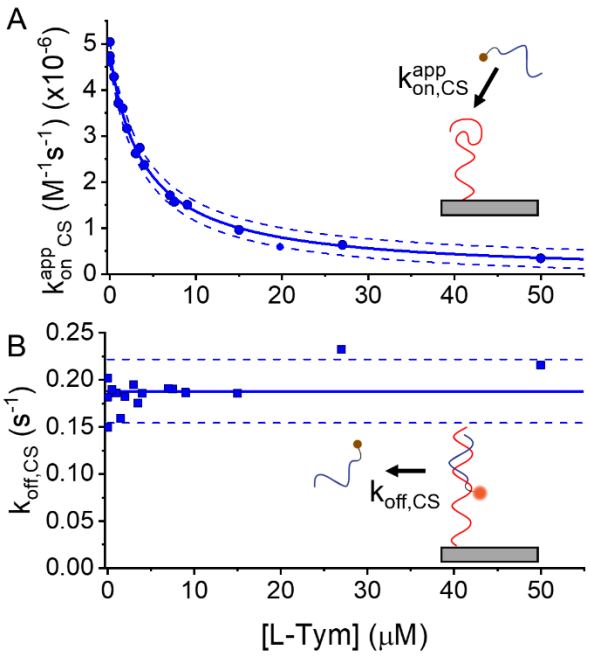

Figure 3. Complementary strand hybridization kinetics at "active" aptamer sites. (A) Average association rates of complementary strand (circle points) from active aptamer population at varying L-Tym concentration. Association rates are fit to the equilibrium model in Equation 4 (solid line). (B) Average dissociation rates at each concentration (square points) with the population average (solid line). Prediction bands at 90% confidence are shown as dashed lines. The relative standard deviation of repeat measurements of $k_{off,CS}$ = 15%, and the relative standard deviation of $k_{on,CS}^{app}$ = 5%.

The model in Equation 4 was fit to $k_{on,CS}^{app}$ data to determine the parameters for $K_{d,LTym}$ and $k_{on,CS}$, as shown by the solid line in Figure 3A. The model predicts $K_{d,LTym}$= 3.9 ± 0.8 μM which is in good agreement with other studies of surface-bound L-Tym aptamers.[36] This model assumes that the complimentary strand cannot bind to the aptamer-L-Tym complex. If this were the case, there would be a non-zero value of $k_{on,CS}^{app}$ at high L-Tym concentrations, corresponding to the association rate of complementary strand with the aptamer-L-Tym complex. We found that a model that incorporates a finite on-rate at high L-Tym did *not* improve the quality of fit, and that the uncertainty in the data would put the upper-bound of that limiting rate at 0.0024 s^{-1}, or only 5% of $k'_{on,CS}$. Additionally, the L-Tym does not invade the aptamer-complementary-strand duplex and induce dissociation; if this were the case, $k_{off,CS}$would increase with L-Tym concentration. We observe no significant trend in $k_{off,CS}$ with [L-Tym], as shown in Figure 3B, indicating that L-Tym does not interact with the complementary-strand-aptamer duplex to induce dissociation. Therefore, the mechanism for the L-Tym aptamer structure-switching biosensor is consistent with an S_N1-like competitive equilibrium (Scheme 1B), and not target-induced strand displacement in the aptamer (Scheme 1A).

Determining the kinetics of L-Tym-aptamer association. Although the trend in $k_{on,CS}^{app}$ in Figure 3A provides the dissociation constant of L-Tym binding to the aptamer, it does not offer insight into L-Tym-aptamer binding kinetics. The dissociation constant for L-Tym binding to the aptamer is the ratio of dissociation and association rates, $K_{d,LTym} = k_{off,LTym}/k_{on,LTym}$; thus, a small dissociation constant could arise from very efficient formation (fast $k_{on,LTym}$) of a relatively weak complex (fast $k_{off,LTym}$), or less inefficient formation (slow $k_{on,LTym}$) of a strongly-bound complex (slow $k_{off,LTym}$). Because L-Tym is not labeled, we cannot directly detect L-Tym binding to the aptamer to determine its kinetics; however, we can observe its effects on the hybridization kinetics of the complementary strand. If the aptamer forms a stable complex with L-Tym that blocks complementary-strand hybridization for long periods of time, the lifetime of the L-Tym-aptamer complex will govern the distribution of time intervals between complementary-strand hybridization events.

In recent work from our lab, we investigated a three-component DNA reaction having a similar mechanism, where fluorescently-labeled and unlabeled DNA in solution compete to hybridize with immobilized probe DNA.[28] We determined the hybridization kinetics of the *unlabeled DNA strand* – which could not be detected directly– by its influence on the labeled

complementary-strand hybridization to the immobilized probe. To do this, we solved the differential equations for the rates of labeled and unlabeled DNA hybridizing competitively with probe DNA to determine a time-domain model that predicts the distribution of time intervals between labeled-strand hybridization events.[28] The same system of differential equations can be applied to model the association of unlabeled L-Tym with the aptamer, $k_{on,LTym}$, its dissociation from the aptamer, $k_{off,LTym}$, and the association rate of the labeled complementary strand with the aptamer, $k_{on,CS}$. The solution to this system of differential equations (Supporting Information) predicts the time-interval distribution of complementary-strand binding events, which is equivalent to the time-decay of the population of free- [A] and L-Tym-bound [LA] aptamers, given by the sum of two exponentials:

$$A(t) + LA(t) = A_{tot}[C_1 e^{-k_1 t} + C_2 e^{-k_2 t}] \qquad \textbf{Equation 5}$$

where

$$k_1 = \frac{k_{off,LTym} + k'_{on,\mathrm{CS}} + k'_{on,LTym} + k_q}{2}$$

$$k_2 = \frac{k_{off,LTym} + k'_{on,\mathrm{CS}} + k'_{on,LTym} - k_q}{2}$$

$$C_1 = \frac{k'_{on,\mathrm{CS}} - k_{off,LTym} - k'_{on,LTym} + k_q}{2k_q}$$

$$C_2 = \frac{k'_{on,CS} - k_{off,LTym} - k'_{on,LTym} - k_q}{2k_q}$$

$$k_q = \sqrt{k^2_{off,LTym} + k'^2_{on,\mathrm{CS}} + k'^2_{on,LTym} - 2k_{off,LTym}k'_{on,RO} + 2k_{off,LTym}k'_{on,LTym} + 2k'_{on,RO}k'_{on,LTym}}$$

where again primes indicate pseudo-first-order on-rates, e.g. $k'_{on,LTym} = k_{on,LTym}\,[LTyr]$.

When the lifetime of the aptamer-L-Tym complex is comparable to the time interval between complementary-strand association events, this model predicts that the distribution of time intervals between complementary-strand hybridization events will shift from a single-exponential decay with no L-Tym in solution, to a double-exponential decay process at high L-Tym concentrations. Histograms of time intervals between complementary-strand hybridization events are generated by pooling the hybridization-event time-intervals measured at all active aptamer molecules. Time intervals are represented as cumulative-survival histograms[45] and are shown for varying L-Tym concentrations in Figure 4A. With no L-Tym in solution, the time intervals between complementary-strand hybridizations are fit well by a single-exponential distribution

consistent with pseudo-first-order kinetics. At higher L-Tym concentrations, the curves deviate significantly from single-exponential behavior, suggesting a long-lived aptamer-L-Tym complex. The competitive kinetic model in Equation 5 was fit to histograms of event intervals for L-Tym concentrations in the range of 0.5-15 μM, with sample data at 1, 3, and 9 μM L-Tym as shown in Figure 4A (with a log-linear plot in Figure S8). L-Tym concentrations above this range exhibited too few hybridization events to effectively sample the interval histogram. The best-fit parameters for $k'_{on,LTym}$ and $k_{off,LTym}$ are plotted in Figures 4B and 4C for each L-Tym concentration. The association rate increases linearly with L-Tym concentration with a zero intercept and slope that represents the association rate constant, $k_{on,LTym}$ = 1.2 ± 0.2 x 10^4 $M^{-1}s^{-1}$. The dissociation rate shows no trend with concentration (least-squares slope is not significantly different from zero), and the L-Tym dissociation rate constant from the average of all data points is $k_{off,LTym}$= 0.045 ± 0.006 s^{-1}. These rate constants predict a $K_{d,LTym}$ = 3.9 ± 0.8 μM, which is indistinguishable from the dissociation constant determined independently from the equilibrium model (Equation 4) fit to the results in Figure 3.

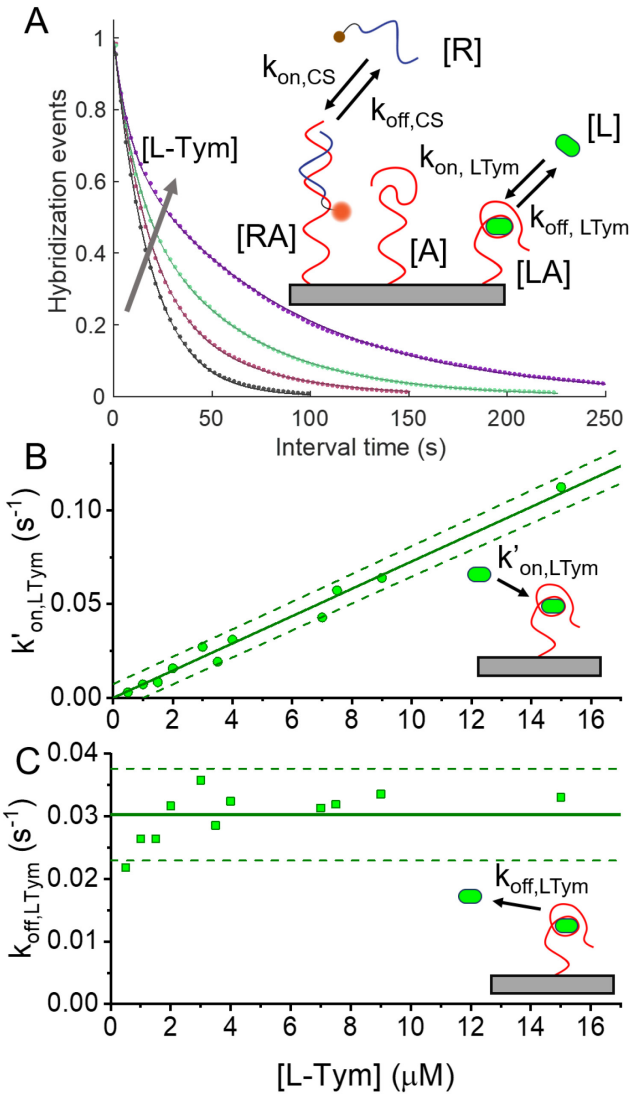

Figure 4. Competitive-binding kinetics of between L-Tym and the complementary strand at aptamer sites. (A) Normalized cumulative histograms of association times between complementary-strand hybridization events at active-aptamer sites at 0 (gray), 1 (pink), 3 (green), and 9 μM (purple) L-Tym with fits to Equation 5 (solid lines). (B) Association on-rates of L-Tym binding to the aptamer at varying L-Tym concentrations (blue points) with a linear-least-squares fit (solid line). (C) Dissociation rates of L-Tym binding (red points) with average rate (solid line). 90% confidence bands are dashed lines.

Investigating the "inactive" aptamer population in a free-solution capture assay. As discussed above, ~30% of the immobilized aptamer molecules exhibit hybridization with the complementary strand but no competitive response to L-Tym. Similar behavior has been observed in DNAzymes,[46] and other structure-switching aptamer biosensors, including those for ochratoxin[47] and dehydroisoandrosterone 3-sulfate[48] where maximum signal is never reached, even at saturating concentrations of

analyte. We cannot provide an explanation for the inactive population, but we have investigated several hypotheses, as discussed in Supporting Information page S10. First, all aptamers were purified by PAGE and HPLC, and the same inactive fraction was observed in independently synthesized samples; this result suggests but does not prove that the inactive population is not due to truncated, chemically modified, or non-deprotected aptamer oligonucleotides. It is possible that this inactive population represents misfolded aptamers that have adopted a structure that is able to hybridize with the complementary strand but is unable to bind to L-Tym. However, our attempt to thermally denature and refold the aptamers in our microscopy flow cell while maintaining individual molecule registration failed to induce interconversion of active and inactive aptamer populations (Figure S9). More extreme temperature and denaturing agents might refold these secondary structures, but we cannot study them *in situ* because these conditions would denature the streptavidin-biotin interaction anchoring the aptamer to the surface. To determine if the heterogeneity is induced by surface immobilization of the aptamer, we immobilized the complementary strand, labeled the aptamer, and performed a competitive pulldown assay to measure the complementary-strand affinity for aptamers in free solution and the dependence on the L-Tym concentration (Figure S10). The results indicate that a similar *30% fraction of the solution-phase aptamer population* is insensitive to L-Tym, showing that this 'inactive' population is not due to surface interactions perturbing the immobilized aptamer.

CONCLUSIONS

The behavior of the structure-switching L-tyrosinamide-binding aptamer investigated in this work is consistent with an S_N1-like mechanism in which the complementary-strand-aptamer duplex must spontaneously dissociate before the aptamer can bind its small-molecule target. The association and dissociation kinetics of the unlabeled L-Tym target were determined based on how their association with the aptamer altered hybridization-interval times of the labeled complementary strand. The exchange kinetics are relatively slow, predicting a long-lived (20s) L-Tym:aptamer complex, and are consistent with dissociation rates measured for L-Tym-binding aptamers in free solution.[36] By probing individual-immobilized aptamer molecules, we determine that a significant (30%) fraction of aptamers have a complementary-strand hybridization response that is insensitive to L-Tym. Other structure-switching aptamer reports have shown that the maximum unquenched fluorescence intensity is not restored even at high concentrations of ligands,[47-48] possibly due to similar fractions of inactive-aptamer molecules.

Although we observe purely competitive S_N1-like behavior in this structure-switching aptamer, the specific sequence of the complementary strand cab impact the binding mechanism, which has implications for engineering biosensors.[17, 19] Duplexed aptamers that operate under an S_N2-like mechanism of target-mediated strand displacement will have lower "sensing" dissociation constants (K_{sens}) since the target can displace the complementary strand rather than waiting for duplexed aptamer to spontaneously dissociate.[2, 17] Monserud et al.[19] studied a duplexed adenosine-binding aptamer using solution-phase FRET and found that the dissociation rate of the fluorescently-labeled aptamer from an immobilized capture strand increased at high concentrations of adenosine target only when the aptamer had a "toehold" region containing the active binding site. The resulting structural change upon target binding to the toehold region induced faster dissociation from the capture DNA. When the active site was hybridized with the capture strand, no displacement was observed, indicating that the target was not able to invade the duplex. Munzar et al.[17] have also shown through competitive equilibrium assays using a duplexed ATP-binding aptamer that the location of the "aptamer-complementary element" determines whether the system exhibits an S_N1 or S_N2-type mechanism. It is likely that the complementary-strand sequence used in this work encompasses the active-site of the aptamer, preventing concerted L-Tym binding and strand displacement. Future single-molecule imaging experiments can address sequence-context and strand-length dependence of S_N1-like versus S_N2-like mechanisms of aptamer kinetics.

It is also notable that the target-aptamer complex has a slow association rate constant ~10^4 $M^{-1}s^{-1}$, which is ~10^5-fold slower than a diffusion-controlled rate (~10^9 $M^{-1}s^{-1}$),[49] along with a slow dissociation rate (lifetime ~20 s). This is consistent with other measurements of small-molecule aptamer association rates, which range from 10^2 to 10^5 $M^{-1}s^{-1}$,[32, 50-51] far below the diffusion-controlled limit. The barrier to target-aptamer complex formation suggests that the target can only associate with a subset of aptamer secondary-structure conformations. M-fold calculations[52] do not predict any stable secondary structures for the L-Tym aptamer sequence, and the sequence is also not a candidate for G-quadruplex formation, suggesting that the aptamer may have to search through a number of random configurations before finding the correct conformation for target binding. Aptamers having more stable stem-loop structures, such as the quinine-binding aptamer,[50] also exhibit inefficient target binding, suggesting a significant barrier to perturb their minimum-energy structure to allow target binding. However, once the target is bound to the aptamer, its configuration is stabilized by a large dissociation barrier, resulting in a slow dissociation rate. This structural rearrangement may be important for the performance of structure-switching aptamers; a

structure insufficiently stabilized by target binding will result in less change in complementary-strand accessibility and stability, resulting in less capacity for target-induced signaling.

The methodology described in this work provides tools to investigate mechanisms of aptamer duplex assembly and target binding, and can be used to study how target binding kinetics, complementary-strand kinetics, and assay sensitivity are affected by the sequence of the complementary strand. Importantly, our approach *does not require labeled analytes*, and thus in principle can be applied to investigations of other aptamer-based sensors or to label-free competition-based studies of ssDNA-binding proteins. These methods can inform the engineering of structure-switching aptamer biosensors to maximize their performance and to provide fundamental insights into molecular interactions with ssDNA.

ACKNOWLEDGEMENTS

This work was supported by the National Science Foundation (CHE-1608949 and CHE-1904380 to J. Harris and CBET-1818476 and CHE-1904885 to J. Heemstra). HHL received funding from the Air Force Institute of Technology Civilian Institute Program. The authors thank Mike Hanson of the University of Utah DNA/Peptide Facility, for oligo synthesis and purification.

Supporting Information Available. Additional information is provided for chemical sources and substrate preparation, the fluorescence microscope, representative single-frame images and single-site trajectories for labeled complementary strand binding, determining a threshold for detecting active-aptamer, distributions of dissociation and hybridization rates at individual aptamer sites, derivation of the competitive-hybridization model, log-linear plot of hybridization interval histograms, characterization of inactive aptamers, and tabulated kinetic results. This material is available free-of-charge via the Internet at http://pubs.acs.org

REFERENCES

1. Dunn, M. R.; Jimenez, R. M.; Chaput, J. C., Analysis of aptamer discovery and technology. *Nat. Rev. Chem.* **2017,** *1*, 0076.

2. Munzar, J. D.; Ng, A.; Juncker, D., Duplexed aptamers: history, design, theory, and application to biosensing. *Chem. Soc. Rev.* **2019,** *48* (5), 1390-1419.

3. Nutiu, R.; Li, Y., Structure-Switching Signaling Aptamers. *J. Am. Chem. Soc.* **2003,** *125* (16), 4771-4778.

4. Chen, J.; Fang, Z.; Liu, J.; Zeng, L., A simple and rapid biosensor for ochratoxin A based on a structure-switching signaling aptamer. *Food Control* **2012,** *25* (2), 555-560.

5. Wickramaratne, T. M.; Pierre, V. C., Turning an Aptamer into a Light-Switch Probe with a Single Bioconjugation. *Bioconjugate Chem.* **2015,** *26* (1), 63-70.

6. Liu, J.; Lu, Y., Fast Colorimetric Sensing of Adenosine and Cocaine Based on a General Sensor Design Involving Aptamers and Nanoparticles. *Angew. Chem. Int. Ed.* **2006,** *45* (1), 90-94.

7. Xiao, Y.; Piorek, B. D.; Plaxco, K. W.; Heeger, A. J., A Reagentless Signal-On Architecture for Electronic, Aptamer-Based Sensors via Target-Induced Strand Displacement. *J. Am. Chem. Soc.* **2005,** *127* (51), 17990-17991.

8. Darmostuk, M.; Rimpelova, S.; Gbelcova, H.; Ruml, T., Current approaches in SELEX: An update to aptamer selection technology. *Biotechnol. Adv.* **2015,** *33* (6, Part 2), 1141-1161.

9. Nutiu, R.; Li, Y., In Vitro Selection of Structure-Switching Signaling Aptamers. *Angew. Chem. Int. Ed.* **2005,** *44* (7), 1061-1065.

10. Sefah, K.; Yang, Z.; Bradley, K. M.; Hoshika, S.; Jiménez, E.; Zhang, L.; Zhu, G.; Shanker, S.; Yu, F.; Turek, D.; Tan, W.; Benner, S. A., In vitro selection with artificial expanded genetic information systems. *Proc. Natl. Acad. Sci. U. S. A.* **2014,** *111* (4), 1449.

11. Meek, K. N.; Rangel, A. E.; Heemstra, J. M., Enhancing aptamer function and stability via in vitro selection using modified nucleic acids. *Methods* **2016,** *106*, 29-36.

12. Rangel, A. E.; Chen, Z.; Ayele, T. M.; Heemstra, J. M., In vitro selection of an XNA aptamer capable of small-molecule recognition. *Nucleic Acids Res.* **2018,** *46* (16), 8057-8068.

13. Ni, S.; Yao, H.; Wang, L.; Lu, J.; Jiang, F.; Lu, A.; Zhang, G., Chemical Modifications of Nucleic Acid Aptamers for Therapeutic Purposes. *Int. J. Mol. Sci.* **2017,** *18* (8).

14. Tolle, F.; Brändle, G. M.; Matzner, D.; Mayer, G., A Versatile Approach Towards Nucleobase-Modified Aptamers. *Angew. Chem. Int. Ed.* **2015,** *54* (37), 10971-10974.

15. Gawande, B. N.; Rohloff, J. C.; Carter, J. D.; von Carlowitz, I.; Zhang, C.; Schneider, D. J.; Janjic, N., Selection of DNA aptamers with two modified bases. *Proc. Natl. Acad. Sci. U. S. A.* **2017,** *114* (11), 2898.

16. Vallée-Bélisle, A.; Ricci, F.; Plaxco, K. W., Engineering Biosensors with Extended, Narrowed, or Arbitrarily Edited Dynamic Range. *J. Am. Chem. Soc.* **2012,** *134* (6), 2876-2879.

17. Munzar, J. D.; Ng, A.; Corrado, M.; Juncker, D., Complementary oligonucleotides regulate induced fit ligand binding in duplexed aptamers. *Chem. Sci.* **2017,** *8* (3), 2251-2256.

18. Feagin, T. A.; Maganzini, N.; Soh, H. T., Strategies for Creating Structure-Switching Aptamers. *ACS Sens.* **2018,** *3* (9), 1611-1615.

19. Monserud, J. H.; Macri, K. M.; Schwartz, D. K., Toehold-Mediated Displacement of an Adenosine-Binding Aptamer from a DNA Duplex by its Ligand. *Angew. Chem. Int. Ed.* **2016,** *55* (44), 13710-13713.

20. Weng, R.; Lou, S.; Li, L.; Zhang, Y.; Qiu, J.; Su, X.; Qian, Y.; Walter, N. G., Single-Molecule Kinetic Fingerprinting for the Ultrasensitive Detection of Small Molecules with Aptasensors. *Anal. Chem.* **2019,** *91* (2), 1424-1431.

21. Chen, J.; Bremauntz, A.; Kisley, L.; Shuang, B.; Landes, C. F., Super-Resolution mbPAINT for Optical Localization of Single-Stranded DNA. *ACS Appl. Mater. Interfaces* **2013,** *5* (19), 9338-9343.

22. Johnson-Buck, A.; Nangreave, J.; Kim, D.-N.; Bathe, M.; Yan, H.; Walter, N. G., Super-Resolution Fingerprinting Detects Chemical Reactions and Idiosyncrasies of Single DNA Pegboards. *Nano Lett.* **2013,** *13* (2), 728-733.

23. Jungmann, R.; Avendano, M. S.; Dai, M.; Woehrstein, J. B.; Agasti, S. S.; Feiger, Z.; Rodal, A.; Yin, P., Quantitative super-resolution imaging with qPAINT. *Nat Meth* **2016,** *13* (5), 439-442.

24. Su, X.; Li, Z.; Yan, X.; Wang, L.; Zhou, X.; Wei, L.; Xiao, L.; Yu, C., Telomerase Activity Detection with Amplification-Free Single Molecule Stochastic Binding Assay. *Anal. Chem.* **2017,** *89* (6), 3576-3582.

25. Yu, Y.; Ma, L.; Li, L.; Deng, Y.; Xu, L.; Liu, H.; Xiao, L.; Su, X., Digestion of Dynamic Substrate by Exonuclease Reveals High Single-Mismatch Selectivity. *Anal. Chem.* **2018,** *90* (22), 13655-13662.

26. Morris, F. D.; Peterson, E. M.; Heemstra, J. M.; Harris, J. M., Single-Molecule Kinetic Investigation of Cocaine-Dependent Split-Aptamer Assembly. *Anal. Chem.* **2018,** *90* (21), 12964-12970.

27. Feagin, T. A.; Olsen, D. P. V.; Headman, Z. C.; Heemstra, J. M., High-Throughput Enantiopurity Analysis Using Enantiomeric DNA-Based Sensors. *J. Am. Chem. Soc.* **2015,** *137* (12), 4198-4206.

28. Peterson, E. M.; Reece, E. J.; Li, W.; Harris, J. M., Super-Resolution Imaging of Competitive Unlabeled DNA Hybridization Reveals the Influence of Fluorescent Labels on Duplex Formation and Dissociation Kinetics. *J. Phys. Chem. B* **2019,** *123* (50), 10746-10756.

29. Peterson, E. M.; Harris, J. M., Identification of Individual Immobilized DNA Molecules by Their Hybridization Kinetics Using Single-Molecule Fluorescence Imaging. *Anal. Chem.* **2018,** *90* (8), 5007-5014.

30. Gooding, J. J.; Gaus, K., Single-Molecule Sensors: Challenges and Opportunities for Quantitative Analysis. *Angew. Chem. Int. Ed.* **2016,** *55* (38), 11354-11366.

31. Johnson-Buck, A.; Li, J.; Tewari, M.; Walter, N. G., A guide to nucleic acid detection by single-molecule kinetic fingerprinting. *Methods* **2019,** *153*, 3-12.

32. Elenko, M. P.; Szostak, J. W.; van Oijen, A. M., Single-Molecule Imaging of an in Vitro-Evolved RNA Aptamer Reveals Homogeneous Ligand Binding Kinetics. *J. Am. Chem. Soc.* **2009,** *131* (29), 9866-9867.

33. Moreira, B. G.; You, Y.; Owczarzy, R., Cy3 and Cy5 dyes attached to oligonucleotide terminus stabilize DNA duplexes: Predictive thermodynamic model. *Biophys. Chem.* **2015,** *198*, 36-44.

34. Peterson, E. M.; Manhart, M. W.; Harris, J. M., Competitive Assays of Label-Free DNA Hybridization with Single-Molecule Fluorescence Imaging Detection. *Anal. Chem.* **2016,** *88* (12), 6410-6417.

35. Mao, X.; Liu, C.; Hesari, M.; Zou, N.; Chen, P., Super-resolution imaging of non-fluorescent reactions via competition. *Nature Chemistry* **2019,** *11* (8), 687-694.

36. Challier, L.; Miranda-Castro, R.; Barbe, B.; Fave, C.; Limoges, B.; Peyrin, E.; Ravelet, C.; Fiore, E.; Labbé, P.; Coche-Guérente, L.; Ennifar, E.; Bec, G.; Dumas, P.; Mavré, F.; Noël, V., Multianalytical Study of the Binding between a Small Chiral Molecule and a DNA Aptamer: Evidence for Asymmetric Steric Effect upon 3′- versus 5′-End Sequence Modification. *Anal. Chem.* **2016,** *88* (23), 11963-11971.

37. Yazawa, K.; Furusawa, H., Probing Multiple Binding Modes of DNA Hybridization: A Comparison between Single-Molecule Observations and Ensemble Measurements. *ACS Omega* **2018,** *3* (2), 2084-2092.

38. Peterson, E. M.; Manhart, M. W.; Harris, J. M., Single-Molecule Fluorescence Imaging of Interfacial DNA Hybridization Kinetics at Selective Capture Surfaces. *Anal. Chem.* **2016,** *88* (2), 1345-1354.

39. Swoboda, M.; Henig, J.; Cheng, H.-M.; Brugger, D.; Haltrich, D.; Plumeré, N.; Schlierf, M., Enzymatic Oxygen Scavenging for Photostability without pH Drop in Single-Molecule Experiments. *ACS Nano* **2012,** *6* (7), 6364-6369.

40. Cooper, D.; Uhm, H.; Tauzin, L. J.; Poddar, N.; Landes, C. F., Photobleaching Lifetimes of Cyanine Fluorophores Used for Single-Molecule Förster Resonance Energy Transfer in the Presence of Various Photoprotection Systems. *ChemBioChem* **2013,** *14* (9), 1075-1080.

41. Johnson-Buck, A.; Walter, N. G., Discovering anomalous hybridization kinetics on DNA nanostructures using single-molecule fluorescence microscopy. *Methods* **2014,** *67* (2), 177-184.

42. Johnson-Buck, A.; Su, X.; Giraldez, M. D.; Zhao, M.; Tewari, M.; Walter, N. G., Kinetic fingerprinting to identify and count single nucleic acids. *Nat Biotech* **2015,** *33* (7), 730-732.

43. Chilkoti, A.; Stayton, P. S., Molecular Origins of the Slow Streptavidin-Biotin Dissociation Kinetics. *J. Am. Chem. Soc.* **1995,** *117* (43), 10622-10628.

44. Yakovchuk, P.; Protozanova, E.; Frank-Kamenetskii, M. D., Base-stacking and base-pairing contributions into thermal stability of the DNA double helix. *Nucleic Acids Res.* **2006,** *34* (2), 564-574.

45. Walder, R.; Kastantin, M.; Schwartz, D. K., High throughput single molecule tracking for analysis of rare populations and events. *Analyst* **2012,** *137* (13), 2987-2996.

46. Carrigan, M. A.; Ricardo, A.; Ang, D. N.; Benner, S. A., Quantitative Analysis of a RNA-Cleaving DNA Catalyst Obtained via in Vitro Selection. *Biochemistry* **2004,** *43* (36), 11446-11459.

47. Tan, Z.; Feagin, T. A.; Heemstra, J. M., Temporal Control of Aptamer Biosensors Using Covalent Self-Caging To Shift Equilibrium. *J. Am. Chem. Soc.* **2016,** *138* (20), 6328-6331.

48. Peterson, A. M.; Jahnke, F. M.; Heemstra, J. M., Modulating the Substrate Selectivity of DNA Aptamers Using Surfactants. *Langmuir* **2015,** *31* (43), 11769-11773.

49. Clegg, R. M., Derivation of diffusion controlled chemical rate constants with the help of Einstein's original derivation of the diffusion constant. *J. Chem. Educ.* **1986,** *63* (7), 571.

50. Bao, J.; Krylova, S. M.; Reinstein, O.; Johnson, P. E.; Krylov, S. N., Label-Free Solution-Based Kinetic Study of Aptamer–Small Molecule Interactions by Kinetic Capillary Electrophoresis with UV Detection Revealing How Kinetics Control Equilibrium. *Anal. Chem.* **2011,** *83* (22), 8387-8390.

51. Chang, A. L.; McKeague, M.; Liang, J. C.; Smolke, C. D., Kinetic and Equilibrium Binding Characterization of Aptamers to Small Molecules using a Label-Free, Sensitive, and Scalable Platform. *Anal. Chem.* **2014,** *86* (7), 3273-3278.

52. Zuker, M., Mfold web server for nucleic acid folding and hybridization prediction. *Nucleic Acids Res.* **2003,** *31* (13), 3406-3415.